Quantum conductivity correction in a two-dimensional disordered pseudospin-1 system

Zhi Yang,[1] Weiwei Chen,[1] Q. W. Shi,[1,2,*] and Qunxiang Li[1,2,†]

[1]*Hefei National Laboratory for Physical Sciences at the Microscale, University of Science and Technology of China, Hefei, Anhui 230026, China*

[2]*Synergetic Innovation Center of Quantum Information and Quantum Physics, University of Science and Technology of China, Hefei, Anhui 230026, China*

(Received 11 December 2018; revised manuscript received 1 March 2019; published 15 April 2019)

Using the Feynman diagram techniques, we theoretically obtain the quantum conductivity correction for a two-dimensional pseudospin-1 electron system in the presence of long-range diagonal disorder. Theoretical results clearly reveal that the quantum correction depends on the sublattice correlation properties of disorder potential. The sublattice correlated disorder gives rise to normal weak localization, while the sublattice uncorrelated impurity potential leads to the absence of logarithmic term in quantum conductivity correction. Remarkably, those results cannot be understood by conventional symmetry classification. An additional symmetry operator involving internal sublattice degrees of freedom, analogous with the time reversal symmetry operator, enables us to clarify our findings from symmetry consideration.

DOI: 10.1103/PhysRevB.99.134204

I. INTRODUCTION

Weak localization originates from the constructive interference between the waves propagating along time-reversed paths. In a conventional two-dimensional (2D) electron gas system, the constructive interference enhances the backscattering amplitudes and causes the negative quantum conductivity correction [1]. Remarkably, this correction diverges logarithmically at low temperatures [2]. Such a divergence provides a precursor of the Anderson localization and reflects universal symmetry properties of the system. Recently, the exploration of the quantum correction for pseudospin-1/2 electron systems (i.e., graphene) is a major activity in current condensed matter physics [3–8]. Due to the nontrivial Berry phase in graphene, the earlier studies showed that quantum correction can be either positive or negative depending on the range of impurity potentials. The long-range disorder only causes intravalley scattering and gives rise to positive quantum correction, while the short-range disorder yields negative contribution owing to the presence of intervalley scattering processes.

Most recently, the low-energy spectrum of the quasiparticles described by the Dirac-Weyl equation with pseudospin-1 have attracted much attention. Electronic materials including $SrCu_2(BO_3)_2$ [9], transition-metal oxide trilayer heterostructure [10], and MoS_2 allotropes with a square symmetry [11] can host such quasiparticles. These pseudospin-1 systems have also been theoretically predicted and experimentally realized on optical dice or Lieb lattices with ultracold atoms [12,13] and particularly engineered photonic crystals [14–16]. Especially the variation of length scale in photonic crystals plays the role of potential change in pseudospin-1 systems. Its unusual spectrum consisting of two graphenelike bands and one additional flat band intersecting with them at the Dirac point implies the emergence of novel electronic properties, such as super Klein tunneling [17], topological localization [18,19], and anomalous Anderson localization behaviors with one-dimensional disorder [20].

However, quantum correction to conductivity for these systems has not been, in our opinion, sufficiently investigated to date. Only a few studies have been devoted to this problem. Vigh *et al.* [21] calculated the semiclassical conductivity in the pseudospin-1 family of Dirac-Weyl fermion. Although the group velocity is vanishing in the flat band where the density of states exhibits a sharp peak, the dc conductivity at the Dirac point still diverges logarithmically with decreasing disorder due to interband transitions between the propagating and the flat bands. Actually, they also indicated that the leading impurity corrections to the current vertex depend on the sublattice correlation of a random potential: The ladder vertex corrections vanish for sublattice uncorrelated disorder but yield finite contribution for sublattice correlated scatterers. However, quantitative analysis and technical details are not provided in their work [21].

In this work, using the Feynman diagram techniques, we systematically study the quantum conductivity of the 2D pseudospin-1 Dirac-Weyl electron system in the presence of long-range diagonal disorder. We show that the ladder vertex correction vanishes for the sublattice uncorrelated scatterers. However, the sublattice correlated scatterers yield finite vertex correction and the transport relaxation time is three times the elastic scattering time. These results are in agreement with that derived from the semiclassical Boltzmann approach. More importantly, we study quantum conductivity correction resulted from quantum interference beyond the semiclassical transport theory. Traditionally, weak localization correction is related to classification of the universality class according to whether the system Hamiltonian has the time reversal and

*Corresponding author: phsqw@ustc.edu.cn
†Corresponding author: liqun@ustc.edu.cn

spin rotation symmetries. Owing to the absence of magnetic impurity scattering or spin-orbit coupling in Hamiltonian, our system should belong to the orthogonal class and give rise to normal weak localization. However, our theoretical results clearly reveal that quantum conductivity correction depends strongly on the sublattice correlation properties of the diagonal disorder. The sublattice correlated scatterers yield normal weak localization, belonging to the orthogonal class. In contrast, the sublattice uncorrelated potentials lead to the absence of logarithmic term for quantum conductivity correction, strongly suggesting that the system should belong to the unitary class even in the absence of magnetic field or magnetic impurity scattering. This seems in contrast with the conventional classification of universality classes. Here, an additional symmetry operator, analogous with the time reversal symmetry operator, is proposed for understanding such interesting findings.

II. MODEL FOR PSEUDOSPIN-1 SYSTEM

The unit cell of the dice lattice consists of a so-called hub site (H) and two rim sites (A and B), and those internal degrees of freedom play the role of a pseudospin-1 system [22,23]. Its Brillouin zone is hexagonal and contains a pair of nodes (or called Dirac points), similar to graphene. The low-energy dynamics near each node can be described by the pseudospin-1 Dirac-Weyl Hamiltonian,

$$H = \hbar v_F \boldsymbol{S}\cdot\boldsymbol{k}, \tag{1}$$

where v_F is the Fermi velocity, $\boldsymbol{k} = (k_x, k_y)$, and

$$S_x = \frac{1}{\sqrt{2}}\begin{pmatrix}0&1&0\\1&0&1\\0&1&0\end{pmatrix}, \quad S_y = \frac{1}{\sqrt{2}}\begin{pmatrix}0&-i&0\\i&0&-i\\0&i&0\end{pmatrix}, \tag{2}$$

combining with

$$S_z = \begin{pmatrix}1&0&0\\0&0&0\\0&0&-1\end{pmatrix}. \tag{3}$$

S_x, S_y form a three-dimensional representation of $SU(2)$, satisfying commutation relation $[S_i, S_j] = i\epsilon_{ijk}S_k$, similar to the Pauli matrix. However, they do not form a Clifford algebra $\{S_i, S_j\} \neq 2\delta_{ij}$. The energy spectrum is isotropic and consists of three branches labeled by the index $s = 0, \pm$, leading to a perfectly flat energy band and two linearly dispersive bands at each node,

$$\varepsilon_s(\boldsymbol{k}) = s\hbar v_F k. \tag{4}$$

The eigenstates in the two branches with $s = \pm$ are expressed as

$$|s\boldsymbol{k}\rangle = \frac{1}{2}\begin{pmatrix}e^{-i\theta}\\ s\sqrt{2}\\ e^{i\theta}\end{pmatrix}\otimes|\boldsymbol{k}\rangle. \tag{5}$$

For the flat band with $s = 0$ they are

$$|0\boldsymbol{k}\rangle = \frac{1}{\sqrt{2}}\begin{pmatrix}e^{-i\theta}\\ 0\\ -e^{i\theta}\end{pmatrix}\otimes|\boldsymbol{k}\rangle, \tag{6}$$

where $e^{i\theta} = (k_x + ik_y)/k$.

To explore disorder effect on conductivity, in this work, we only consider the long-range disorder whose potential range is larger than the lattice constant. This assumption allows us to neglect the scattering between the pair of nodes [24].

III. RESULTS AND DISCUSSION

A. Sublattice correlated disorder

First, we start with the Gaussian disorder with sublattice correlation,

$$U = V(\boldsymbol{r})I, \tag{7}$$

and

$$\overline{V(\boldsymbol{r})V(\boldsymbol{r}')} = \gamma\delta(\boldsymbol{r}-\boldsymbol{r}'). \tag{8}$$

Here, $\overline{\cdots}$ denotes the average over disorder realization, the parameter γ quantifies the disorder strength, and I is the identity matrix of rank 3. The using of δ function is based on the assumption that the potential range is much smaller than the varying range of the wave function.

Within the lowest Born approximation, the elastic scattering time is defined by

$$\frac{1}{\tau_s} = \frac{2\pi}{\hbar}\sum_{s'k'}\overline{|\langle s\boldsymbol{k}|U|s'\boldsymbol{k}'\rangle|^2}\delta(\varepsilon_F - \varepsilon_{s'}(\boldsymbol{k})). \tag{9}$$

Using Eqs. (7)–(9), the elastic scattering times in branches with $s = \pm 1$ are found to be equivalent:

$$\frac{1}{\tau_+} = \frac{1}{\tau_-} = \frac{3\varepsilon_F\gamma}{8\hbar^3 {v_F}^2} = \frac{1}{\tau}. \tag{10}$$

Here, the Fermi energy ε_F is assumed to be large enough to satisfy the weak scattering limit $\varepsilon_F\tau \gg 1$. In this regime, the elastic scattering time calculated by the lowest Born approximation is in agreement with that derived from self-consistent Born approximation [21]. This agreement reflects that the transition between different branches can be neglected. In the following calculations, therefore, we can fix the branch index s to be "+" and treat the spectral function as a delta function approximately [25].

We calculate conductivity by the Kubo formula. Under Drude approximation, the classical Drude conductivity is calculated by only considering the contribution from the bubble diagram shown in Fig. 1(a),

$$\sigma_{\text{Drude}} = \frac{\hbar}{2\pi}\int\frac{d\boldsymbol{k}}{(2\pi)^2}j^x(\boldsymbol{k})G^+(\boldsymbol{k})j^x(\boldsymbol{k})G^-(\boldsymbol{k}), \tag{11}$$

where $j^x(\boldsymbol{k}) = ev_F\langle+\boldsymbol{k}|S_x|+\boldsymbol{k}\rangle = ev_F\cos\theta$ denotes the electric current operator and the disorder averaged Green's function is defined as $G^\pm = 1/(\varepsilon_F - \hbar v_F k \pm i\hbar/2\tau)$. From Eq. (11) we express the Drude conductivity as

$$\sigma_{\text{Drude}} = \frac{e^2}{4\pi\hbar}\frac{\varepsilon_F\tau}{\hbar}. \tag{12}$$

As we see, the conductivity of Dirac-Weyl fermion with pseudospin-1 within the Drude approximation is similar to that of graphene [3,26]. Physically, the similar conelike bands structure is the simple reason to hold the same Drude conductivity expression for both systems.

Commonly, the leading multiple scattering is described by ladder vertex correction as shown in Fig. 1(b), and the

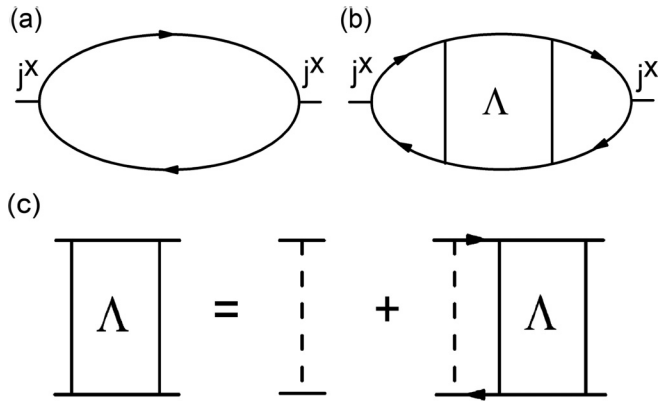

FIG. 1. Diagrams for calculations of conductivity by Kubo formula: (a) Drude approximation, (b) the vertex correction, and (c) the Bethe-Salpeter equation for vertex function Λ. A solid line with an arrow denotes an averaged Green function. A dashed line represents a bare vertex function.

corresponding contribution to the conductivity is given by

$$\sigma_D = \frac{\hbar}{2\pi}\int \frac{d\boldsymbol{k}d\boldsymbol{k}'}{(2\pi)^4} j^x(\boldsymbol{k}) j^x(\boldsymbol{k}') \times G^+(\boldsymbol{k})G^-(\boldsymbol{k})\Lambda(\boldsymbol{k},\boldsymbol{k}')G^-(\boldsymbol{k}')G^+(\boldsymbol{k}'). \quad (13)$$

The vertex-part $\Lambda(\boldsymbol{k},\boldsymbol{k}')$ satisfies the Bethe-Salpeter equation, diagrammatically represented by Fig. 1(c),

$$\Lambda(\boldsymbol{k},\boldsymbol{k}') = \Lambda^0(\boldsymbol{k},\boldsymbol{k}') + \int \frac{d\boldsymbol{q}}{(2\pi)^2}\Lambda^0(\boldsymbol{k},\boldsymbol{q})G^+(\boldsymbol{q})G^-(\boldsymbol{q})\Lambda(\boldsymbol{q},\boldsymbol{k}'), \quad (14)$$

where the bare vertex

$$\Lambda^0(\boldsymbol{k},\boldsymbol{k}') = \overline{|\langle +\boldsymbol{k}|U|+\boldsymbol{k}'\rangle|^2} = \frac{\gamma}{4}[1+cos(\theta-\theta')]^2. \quad (15)$$

Before trying to solve Eq. (13) iteratively, we notice that the vertex function shows angular dependence and totally suppresses the backscattering process. To retain the isotropy of system, we only keep those parts of vertex functions with $e^{\pm i(\theta-\theta')}$. To this end, $\Lambda^0(\boldsymbol{k},\boldsymbol{k}') = \frac{\gamma}{4}[e^{-i(\theta-\theta')}+e^{i(\theta-\theta')}]$. Substituting the bare vertex function into Eq. (14), we obtain the vertex function

$$\Lambda(\boldsymbol{k},\boldsymbol{k}') = \frac{3\gamma}{4}[e^{-i(\theta-\theta')}+e^{i(\theta-\theta')}], \quad (16)$$

and immediately the ladder vertex contribution to conductivity equals to

$$\sigma_D = \frac{e^2}{2\pi\hbar}\frac{\varepsilon_F\tau}{\hbar}. \quad (17)$$

The total semiclassical conductivity $\sigma = \sigma_{\text{Drude}} + \sigma_D$ can be expressed as

$$\sigma = \frac{e^2}{4\pi\hbar}\frac{\varepsilon_F\tau_{tr}}{\hbar} = \frac{e^2}{4\pi\hbar}k_F l, \quad (18)$$

where the transport relaxation time $\tau_{tr} = 3\tau$, Fermi velocity $k_F = \varepsilon_F/\hbar v_F$, and $l = v_F\tau_{tr}$ denotes the transport relaxation length. In other words, the conductivity triples and the transport relaxation time τ_{tr} is three times the scattering time τ. This is different from in graphene, where the conductivity just doubles due to the ladder vertex correction [3,26,27].

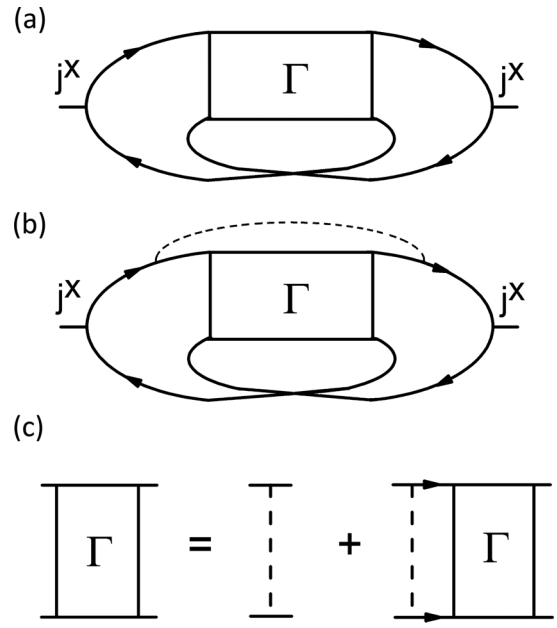

FIG. 2. The diagrams for the coherent scattering corrections to conductivity: (a) the Cooperon correction, (b) the nonbackscattering contribution (the dressed Hikami boxes), (c) the Bethe-Salpeter equation for vertex function Γ. A solid line with an arrow denotes an averaged Green function. A dashed line represents a bare vertex function.

Now we turn to study the quantum correction to the total semiclassical conductivity, which results from interference processes between electrons passing along the time-reversed paths, leading to the weak localization or weak antilocalization. As illustrated in Fig. 2(a), the sum of all such diagrams is called a "Cooperon," owing to its similarity to the pair susceptibility in superconductivity. The quantum conductivity correction is thus given by

$$\sigma_C = \frac{\hbar}{2\pi}\int \frac{d\boldsymbol{k}d\boldsymbol{k}'}{(2\pi)^4} j^x(\boldsymbol{k}) j^x(\boldsymbol{k}') \times G^+(\boldsymbol{k})G^-(\boldsymbol{k})\Gamma(\boldsymbol{k}+\boldsymbol{k}')G^-(\boldsymbol{k}')G^+(\boldsymbol{k}'). \quad (19)$$

This expression is analog to that in the vertex correction, but the Cooperon $\Gamma(\boldsymbol{q}=\boldsymbol{k}+\boldsymbol{k}')$ has a peak at backscattering $\boldsymbol{q}=0$. Under the condition $q\to 0$, the bare vertex of Cooperon is given by

$$\Gamma^0(\boldsymbol{k},\boldsymbol{k}';\boldsymbol{q}) = \frac{3\gamma}{8} + \frac{\gamma}{4}[e^{-i(\theta-\theta')}+e^{i(\theta-\theta')}] + \frac{\gamma}{16}[e^{-i2(\theta-\theta')}+e^{i2(\theta-\theta')}]. \quad (20)$$

The form of Cooperon Γ can be assumed to be [28,29]

$$\Gamma(\boldsymbol{k},\boldsymbol{k}';\boldsymbol{q}) = \sum_{n,m=-2}^{2}\Gamma_{nm}e^{i(n\theta-m\theta')}. \quad (21)$$

Solving the Bethe-Salpeter equation

$$\Gamma(\boldsymbol{k},\boldsymbol{k}';\boldsymbol{q}) = \Gamma^0(\boldsymbol{k},\boldsymbol{k}';\boldsymbol{q}) + \int \frac{d\boldsymbol{p}}{(2\pi)^2}\Gamma^0(\boldsymbol{k},\boldsymbol{p};\boldsymbol{q})G^+(\boldsymbol{p}) \times G^-(\boldsymbol{q}-\boldsymbol{p})\Gamma(\boldsymbol{p},\boldsymbol{k}';\boldsymbol{q}), \quad (22)$$

we only keep the divergent part in the limit $q \to 0$ (see in Appendix A)

$$\Gamma(\boldsymbol{k},\boldsymbol{k}';\boldsymbol{q}) = \frac{3\gamma}{8}\frac{1}{Dq^2\tau}, \tag{23}$$

where $D = v_F^2\tau_{tr}/2$ denotes the diffusion coefficient. Notice that the phase factors disappear here, and this causes a positive vertex function. Consequently the contribution of the Cooperon to conductivity is calculated as

$$\sigma_C = -\frac{3e^2}{4\pi^2\hbar}\ln\frac{\tau_\phi}{\tau}. \tag{24}$$

Here we multiply by $(\tau_{tr}/\tau)^2$ to take into account the correction to velocity from the ladder diagram depicted in Fig. 1(b).

The correction from the Cooperon is negative, showing normal weak localization. Here, we introduce the phase coherence time τ_ϕ as cutoff of integration [30]. At low temperature, the dephasing is dominated by inelastic electron-electron collisions. One can probe dephasing processes by measuring the temperature dependence of conductivity in the weak localization regime [1]. Notice that this negative quantum correction to conductivity in Eq. (24) is in contrast to that in graphene, which is revealed to be positive. The simple explanation is ascribed to the trivial Berry phase in the pseudospin-1 Dirac-Weyl system [20,31], leading to normal weak localization.

The full correction to the conductivity should take into account the nonbackscattering contribution [32–34]. The backscattering and the nonbackscattering contributions to the conductivity are reported to have the same order of magnitude and different signs in 2D systems with large Rashba splitting [30]. The nonbackscattering contribution is given by the diagram in Fig. 2(b) and the other conjugated to it (the dressed Hikami boxes). The corresponding expression reads as

$$\begin{aligned}\sigma_{\text{non-bs}} = 2\frac{\hbar}{2\pi}\int \frac{d\boldsymbol{k}d\boldsymbol{k}'d\boldsymbol{q}}{(2\pi)^6}&\Gamma^0(\boldsymbol{k},-\boldsymbol{k}')j^x(\boldsymbol{k})j^x(\boldsymbol{k}')\\ &\times G^+(\boldsymbol{k})G^-(\boldsymbol{k})G^+(\boldsymbol{k}')G^-(\boldsymbol{k}')\\ &\times G^+(\boldsymbol{q}-\boldsymbol{k})G^+(\boldsymbol{q}-\boldsymbol{k}')\Gamma(\boldsymbol{q}),\end{aligned} \tag{25}$$

where the overall factor of 2 stems from the fact that the diagram conjugated to Fig. 2(b) gives identical contribution. The bare vertex Γ^0 is anisotropic and the average of the angular part is nonzero (see in Appendix B for details). After some algebra, we find that the nonbackscattering contribution to the conductivity takes the form

$$\sigma_{\text{non-bs}} = -\tfrac{2}{3}\sigma_C. \tag{26}$$

This result is similar to that in graphene but their coefficients are different [6]. Finally, the total weak localization correction to the conductivity is obtained

$$\sigma_{WL} = \frac{1}{3}\sigma_C = -\frac{e^2}{4\pi^2\hbar}\ln\frac{\tau_\phi}{\tau}. \tag{27}$$

B. Sublattice uncorrelated disorder

Next, we consider a similar long-range disorder but without sublattice correlation,

$$U' = \sum_{i=1,2,3} V_i(\boldsymbol{r})U_i = \begin{pmatrix} V_1(\boldsymbol{r}) & 0 & 0\\ 0 & V_2(\boldsymbol{r}) & 0\\ 0 & 0 & V_3(\boldsymbol{r})\end{pmatrix}, \tag{28}$$

where $U_i = \text{diag}(\delta_{i1},\delta_{i2},\delta_{i3})$ are projections onto the sublattice A, H, and B, respectively, and $\overline{V_i(\boldsymbol{r})V_j(\boldsymbol{r}')} = \gamma\delta_{ij}\delta(\boldsymbol{r}-\boldsymbol{r}')$. Unlike the sublattice correlated disorder, here the Kronecker delta δ_{ij} emphasizes the independence of disorder potential on different sublattice sites.

The elastic scattering time τ' is determined by Eq. (9) and equals to the one under sublattice uncorrelated disorder: $\tau' = \tau$. However, based on diagrams in Fig. 1 we find that the ladder vertex corrections give no contribution, in contrast to that in sublattice correlated disorder. This is because for the sublattice uncorrelated disorder, the bare vertex function is written as

$$\Lambda'^0(\boldsymbol{k},\boldsymbol{k}') = \overline{\sum_{i=1,2,3}|\langle+\boldsymbol{k}|U_i|+\boldsymbol{k}'\rangle|^2} = \frac{3}{8}\gamma, \tag{29}$$

which is angular independent. Thus the vertex function $\Lambda'(\boldsymbol{k},\boldsymbol{k}')$ is also angular independent and does not depend on the incoming and outgoing directions. Since the current operator $j^x(\boldsymbol{k}) = ev_F\cos\theta$ is the only term that contains an angular part, the angular average in Eq. (13) cancels and the vertex correction to conductivity is zero.

As for the coherent scattering processes in the Cooperon, the bare vertex function with sublattice uncorrelated disorder is different from the one in Eq. (20):

$$\begin{aligned}\Gamma'^0(\boldsymbol{k},\boldsymbol{k}';\boldsymbol{q}) &= \overline{\sum_{i=1,2,3}\langle+\boldsymbol{k}|U_i|+\boldsymbol{k}'\rangle\langle+(-\boldsymbol{k})|U_i|+(-\boldsymbol{k}')\rangle}\\ &= \frac{\gamma}{4}+\frac{\gamma}{16}[e^{-2i(\theta-\theta')}+e^{2i(\theta-\theta')}].\end{aligned} \tag{30}$$

Thus only the zeroth and second angular harmonics remains in the bare vertex. The vertex function $\Gamma'(\boldsymbol{k},\boldsymbol{k}';\boldsymbol{q})$ can be derived from the Bethe-Salpeter equation, however the divergence is absent (see in Appendix A). For example, the expansion coefficients of the zeroth and second angular harmonics take the form, respectively,

$$\Gamma'_{0,0} \approx \frac{9\gamma}{8}\frac{1}{3/2+Dq^2\tau}, \quad \Gamma'_{\pm2,\pm2} \approx \frac{9\gamma}{8}\frac{1}{15+Dq^2\tau}. \tag{31}$$

Thus the vertex function $\Gamma'(\boldsymbol{k},\boldsymbol{k}';\boldsymbol{q})$ has no diffusion pole, which is similar to that in 2D electron gas with magnetic impurities. The absence of diffusion pole in the Cooperon vertex function leads to the absence of the logarithmic term, thus we obtain a vanishing coherent correction to the conductivity under sublattice uncorrelated disorder:

$$\sigma'_C = 0. \tag{32}$$

This is our central finding of this work, indicating that the leading quantum correction to conductivity is absent and our system in this case should belong to the unitary class from symmetry consideration. This result is in sharp contrast with conventional classification of universality classes, since in our

calculation we do not introduce external magnetic field or magnetic impurity scattering. The system Hamiltonian still keeps the time reversal symmetry and should belong to the orthogonal class. The time reversal symmetry operator of the dice lattice $\mathcal{T}_{\rm dice}$ is given by the complex-conjugation operator $\mathcal{C}$. In the low-energy effective Hamiltonian, since the Bloch functions at different nodes are complex conjugate, we have $\mathcal{T}_{\rm dice} = (\sigma_x \otimes I)\mathcal{C}$, where the Pauli matrices σ_x represent the node index.

Note that this time reversal operator commutes with both sublattice correlated and uncorrelated disorder potential. In the absence of internode scattering, however, $\mathcal{T}_{\rm dice}$ cannot be used to classify the universality class for weak localization. Here, we introduce another symmetry operator at each node for classification of universality class,

$$\mathcal{T} = e^{-i\pi S_y}\mathcal{C} = \left(1 - 2S_y^2\right)\mathcal{C}. \tag{33}$$

This operator $\mathcal{T}$ transforms $|s\boldsymbol{k}\rangle$ into $|s{-}\boldsymbol{k}\rangle$ at each node and can be regarded as the time reversal operator for transport under intranode scattering. It is easy to verify that $\mathcal{T}^2 = 1$ and $\mathcal{T}S_i\mathcal{T}^{-1} = -S_i$, $(i = x, y, z)$. Obviously, the original Hamiltonian Eq. (1) is invariant under $\mathcal{T}$ transformation,

$$\mathcal{T}H(-\boldsymbol{k})\mathcal{T}^{-1} = H(\boldsymbol{k}). \tag{34}$$

In the presence of the sublattice correlated disorder we considered above $U = V(\boldsymbol{r})I$, the symmetry $\mathcal{T}$ is retained. Therefore, the disordered system is still orthogonal and the coherent processes of coherent scattering processes give rise to normal weak localization. As for the sublattice uncorrelated disorder in Eq. (28), its formula can be expressed as $U' = V_1(\boldsymbol{r})\frac{1}{2}(S_z^2 + S_z) + V_2(\boldsymbol{r})(1 - S_z^2) + V_3(\boldsymbol{r})\frac{1}{2}(S_z^2 - S_z)$. The uncorrelated parts V_1, V_3 break down the symmetry $\mathcal{T}$, resulting in the absence of the leading quantum correction to conductivity. It should be emphasized that the unitary class, the absence of the logarithmic term, can be realized even in the absence of magnetic impurity scattering. Moreover, interpreting the internal sublattice degrees of freedom as a fictitious spin-1, the origin of the absence of the logarithmic term can be traced back to the term V_1 and V_3, acting as fictitious magnetic impurity scattering.

IV. SUMMARY

In summary, the quantum conductivity of the Dirac-Weyl fermions with pseudospin-1 is calculated in the weak scattering limit. It is found that the ladder vertex and quantum vertex correction strongly depend on the sublattice correlation properties of disorder potential. More importantly, combining previous studies in graphene (pseudospin-1/2 systems) with our investigation on the pseudospin-1 system, we verify that a type of symmetry operator involving internal sublattice degrees of freedom plays an essential role in classifying the universality class associated with the quantum conductivity correction. These predictions can be easily tested in certain photonic crystals. The sublattice correlation properties can be modulated by varying the length scale in photonic crystals [20,35]. Therefore, the sublattice correlated disorder gives rise to a sharp peak of the reflection coefficient in the backscattering direction, as a direct experimental evidence of normal weak localization [36]. However, the sublattice uncorrelated disorder will strongly suppress the peak of reflection coefficient.

ACKNOWLEDGMENTS

We thank the anonymous referee for his/her critical and professional comments. We thank Bo Fu and Wei Zhu for helpful discussions. This work was supported by National Key Research & Development Program of China (Grants No. 2016YFA0200600 and No. 2017YFA0204904), and by the National Natural Science Foundation of China (Grants No. 11874337, No. 11634011, and No. 21873088). Computational resources are provided by Chinese Academy of Sciences, Shanghai and USTC Supercomputer Centers.

APPENDIX A: CALCULATION OF THE COOPERON

Expanding the Green's functions up to q^2 and integrating the product of Green's functions in the Bethe-Salpeter equation (22) over $|\boldsymbol{p}|$, we obtain

$$\int \frac{pdp}{2\pi} G^+(\boldsymbol{p})G^-(\boldsymbol{q}-\boldsymbol{p}) \approx \sum_{n=-2}^{2} \Delta_n e^{in\theta_q}. \tag{A1}$$

Here

$$\begin{aligned}
\Delta_0 &= \frac{\epsilon_F \tau}{\hbar^3 v_F^2}\left(1 - \frac{Q^2}{2}\right),\\
\Delta_{\pm 1} &= -i\frac{\epsilon_F \tau}{\hbar^3 v_F^2}\frac{Q_\mp}{2},\\
\Delta_{\pm 2} &= -\frac{\epsilon_F \tau}{\hbar^3 v_F^2}\frac{Q_\mp^2}{4},
\end{aligned} \tag{A2}$$

where $Q = v_F \tau q$ and $Q_\pm = Qe^{\pm i\theta_q}$. Substituting Eq. (A1) into Eq. (22), we arrive at

$$\begin{aligned}
\Gamma(\boldsymbol{k}, \boldsymbol{k}'; \boldsymbol{q}) &= \Gamma^0(\boldsymbol{k}, \boldsymbol{k}'; \boldsymbol{q})\\
&\quad + \sum_{n=-2}^{2} \int \frac{d\theta_p}{2\pi} \Gamma^0(\boldsymbol{k}, \boldsymbol{p}; \boldsymbol{q})\Gamma(\boldsymbol{p}, \boldsymbol{k}'; \boldsymbol{q})\Delta_n e^{in\theta_p}.
\end{aligned} \tag{A3}$$

Meanwhile, the bare vertex of the Cooperon function under the sublattice correlated disorder can be rewritten as

$$\Gamma^0(\boldsymbol{k}, \boldsymbol{k}'; \boldsymbol{q}) = \sum_{n,m=-2}^{2} \Gamma_n^0 \delta_{nm} e^{i(n\theta - m\theta')}, \tag{A4}$$

where

$$\Gamma_0^0 = \frac{3\gamma}{8}, \quad \Gamma_{\pm 1}^0 = \frac{\gamma}{4}, \quad \Gamma_{\pm 2}^0 = \frac{\gamma}{16}. \tag{A5}$$

Substituting Eqs. (21) and (A4) into Eq. (A3), we get

$$\Gamma_{nm} = \Gamma_n^0 \delta_{nm} + \sum_l \Gamma_n^0 \Delta_{n-l} \Gamma_{lm}. \tag{A6}$$

By defining matrix $\mathbf{\Gamma} = [\Gamma_{nm}]$, $\mathbf{\Gamma^0} = [\Gamma_n^0 \delta_{nm}]$, and $\mathbf{\Delta} = [\Delta_{n-m}]$, we arrive at

$$\mathbf{\Gamma} = \mathbf{\Gamma^0} + \mathbf{\Gamma^0 \Delta \Gamma}, \tag{A7}$$

and the solution is found as

$$\mathbf{\Gamma} = (\mathbf{1} - \mathbf{\Gamma^0 \Delta})^{-1} \mathbf{\Gamma^0}. \tag{A8}$$

The solution can be simplified as

$$\mathbf{\Gamma} = \frac{3\gamma}{8} \begin{bmatrix} 5+\frac{Q^2}{2} & i\frac{Q_+}{2} & \frac{Q_+^2}{4} & 0 & 0 \\ i\frac{Q_-}{2} & \frac{1}{2}+\frac{Q^2}{2} & i\frac{Q_+}{2} & \frac{Q_+^2}{4} & 0 \\ \frac{Q_-^2}{4} & i\frac{Q_-}{2} & \frac{Q^2}{2} & i\frac{Q_+}{2} & \frac{Q_+^2}{4} \\ 0 & \frac{Q_-^2}{4} & i\frac{Q_-}{2} & \frac{1}{2}+\frac{Q^2}{2} & i\frac{Q_+}{2} \\ 0 & 0 & \frac{Q_-^2}{4} & i\frac{Q_-}{2} & 5+\frac{Q^2}{2} \end{bmatrix}^{-1}. \tag{A9}$$

The zeroth angular harmonic is the only divergent part and reads as

$$\Gamma_{00} \approx \frac{3\gamma}{8}\frac{2}{3Q^2} = \frac{3\gamma}{8}\frac{1}{Dq^2\tau}, \tag{A10}$$

where $D = v_F^2\tau_{tr}/2$ denotes the diffusion coefficient. The other diagonal elements are regular: $\Gamma_{\pm1,\pm1} \approx \frac{10\gamma}{69}\frac{1}{20/69+Dq^2\tau}$ and $\Gamma_{\pm2,\pm2} \approx \frac{9\gamma}{10}\frac{1}{12+Dq^2\tau}$. Notice that the Cooperon will be three times overestimated if one neglects the off-diagonal terms in Eq. (A9).

The cooperon under the sublattice uncorrelated disorder can be derived with a similar procedure. The integration in Eq. (A1) is unchanged in this case. But the bare vertex Γ'^0 is different and can be written as

$$\Gamma'^0_0 = \frac{\gamma}{4}, \quad \Gamma'^0_{\pm1} = 0, \quad \Gamma'^0_{\pm2} = \frac{\gamma}{16}. \tag{A11}$$

Notice that the coefficient of zeroth angular harmonic $\Gamma'^0_0 = \frac{\gamma}{4}$ is different from that in sublattice correlated disorder $\Gamma^0_0 = \frac{3\gamma}{8}$, which plays a dominant role in yielding the diffusion pole of the Cooperon. The solution of the corresponding Bethe-Salpeter equation can be expressed as

$$\mathbf{\Gamma'} = \begin{bmatrix} \frac{5}{6}+\frac{Q^2}{12} & i\frac{Q_+}{12} & \frac{Q_+^2}{24} & 0 & 0 \\ 0 & 1 & 0 & 0 & 0 \\ \frac{Q_-^2}{6} & i\frac{Q_-}{3} & \frac{1}{3}+\frac{Q^2}{3} & i\frac{Q_+}{3} & \frac{Q_+^2}{6} \\ 0 & 0 & 0 & 1 & 0 \\ 0 & 0 & \frac{Q_-^2}{24} & i\frac{Q_-}{12} & \frac{5}{6}+\frac{Q^2}{12} \end{bmatrix}^{-1} \mathbf{\Gamma'^0}. \tag{A12}$$

In this case, the divergence in the limit $q \to 0$ is absent, because $\Gamma'_{0,0} \approx \frac{9\gamma}{8}\frac{1}{3/2+Dq^2\tau}$, $\Gamma'_{\pm1,\pm1} = 0$, and $\Gamma'_{\pm2,\pm2} \approx \frac{9\gamma}{8}\frac{1}{15+Dq^2\tau}$. Thus the Cooperon under sublattice uncorrelated disorder has no diffusion pole, and the weak localization is absent in this case.

APPENDIX B: CALCULATION OF THE NONBACKSCATTERING CONTRIBUTION TO THE CONDUCTIVITY

Using the identity

$$G^+(\boldsymbol{k})G^-(\boldsymbol{k}) = \frac{\tau}{i\hbar}[G^-(\boldsymbol{k}) - G^+(\boldsymbol{k})], \tag{B1}$$

and neglecting the rapidly oscillating products of the Green's function, the nonbackscattering contribution can be expressed as

$$\sigma_{\text{non-bs}} = -\frac{\tau^2}{\pi\hbar}\int \frac{d\boldsymbol{k}d\boldsymbol{k}'d\boldsymbol{q}}{(2\pi)^6}\Gamma^0(\boldsymbol{k},-\boldsymbol{k}')j^x(\boldsymbol{k})j^x(\boldsymbol{k}') \times G^-(\boldsymbol{k})G^-(\boldsymbol{k}')G^+(\boldsymbol{q}-\boldsymbol{k})G^+(\boldsymbol{q}-\boldsymbol{k}')\Gamma(\boldsymbol{q}). \tag{B2}$$

Notice that the current operator $j^x(\boldsymbol{k}) = ev_F\cos\theta_{\boldsymbol{k}}$ takes a form similar to that of 2D electron gas. The bare vertex $\Gamma^0(\boldsymbol{k},-\boldsymbol{k}')$ can be derived from Eq. (20),

$$\Gamma^0(\boldsymbol{k},-\boldsymbol{k}') = \frac{\gamma}{4}[1-\cos(\theta-\theta')]^2. \tag{B3}$$

Neglecting $\boldsymbol{q}$ in the Green's functions and taking the average of the angular part, we arrive at

$$\sigma_{\text{non-bs}} = -\frac{e^2{v_F}^2\tau^2}{\pi\hbar}\frac{\gamma}{8}\int\frac{d\boldsymbol{k}d\boldsymbol{k}'}{(2\pi)^4} \times G^-(\boldsymbol{k})G^+(\boldsymbol{k})G^-(\boldsymbol{k}')G^+(\boldsymbol{k}')\int\frac{d\boldsymbol{q}}{(2\pi)^2}\Gamma(\boldsymbol{q}). \tag{B4}$$

Notice that the correction to velocity has not been taken into account, so we need to multiply by $(\tau_{tr}/\tau)^2$. After integrating the Cooperon and the product of the Green functions, we obtain

$$\sigma_{\text{non-bs}} = \frac{e^2}{2\pi^2\hbar}\ln\frac{\tau_\phi}{\tau} = -\frac{2}{3}\sigma_C. \tag{B5}$$

APPENDIX C: TRANSPORT RELAXATION TIME IN BOLTZMANN APPROACH

To gain more physical insight of the above results, we also calculate the transport relaxation time within a standard semiclassical Boltzmann approach. Considering that the system is isotropic, the transport relaxation time in this regime is defined by

$$\frac{1}{\tau_{tr}} = \frac{2\pi}{\hbar}\sum_{k'}\overline{|\langle+\boldsymbol{k}|U|+\boldsymbol{k}'\rangle|^2}\delta(\varepsilon_F-\varepsilon_+(\boldsymbol{k}'))(1-cos\theta'). \tag{C1}$$

In the presence of sublattice correlated disorder, substituting the definition of τ into Eq. (C1) we obtain

$$\tau_{tr} = 3\tau, \tag{C2}$$

which yields the same result as that calculated by using the Kubo formula. Physically, the difference between transport relaxation time and the relaxation time in Green's function originates from the weighting factor $1-\cos\theta'$. The factor tends to favor large-angle scattering events and suppress the small-angle scattering. However, the large-angle scattering will be suppressed by the wave function overlap factor $(1+\cos\theta')^2$. In fact, the transport relaxation time is weighted by an effective angular factor $(1-\cos\theta')(1+\cos\theta')^2$, which suppresses both large- and small-angle scattering contributions. This special angular factor leads to a significant difference between Dirac-Weyl fermions with spin-1 and graphene or 2D electron gas with respect to the behavior of τ_{tr}/τ [27]. On the other hand, the conductivities within the ladder diagrams from the Kubo formula and Boltzmann approach are equivalent in the weak-disorder limit. Indeed this equivalence has

been also noticed in the electron gas with Rashba spin-orbit coupling [25].

As for the sublattice uncorrelated disorder, the special form of disorder yields an angular free wave function overlap factor, and the small-angle scattering will not be suppressed by the weighting factor $1-\cos\theta'$ anymore. This is similar to the case in conventional 2D electron gas, where the isotropic collisions do not yield the vertex contribution to conductivity. Thus we obtain a vanishing ladder vertex correction to conductivity under sublattice uncorrelated disorder.

[1] G. Bergmann, Phys. Rep. **107**, 1 (1984).
[2] T. Ando, A. B. Fowler, and F. Stern, Rev. Mod. Phys. **54**, 437 (1982).
[3] H. Suzuura and T. Ando, Phys. Rev. Lett. **89**, 266603 (2002).
[4] D. V. Khveshchenko, Phys. Rev. Lett. **97**, 036802 (2006).
[5] S. V. Morozov, K. S. Novoselov, M. I. Katsnelson, F. Schedin, L. A. Ponomarenko, D. Jiang, and A. K. Geim, Phys. Rev. Lett. **97**, 016801 (2006).
[6] E. McCann, K. Kechedzhi, V. I. Fal'ko, H. Suzuura, T. Ando, and B. L. Altshuler, Phys. Rev. Lett. **97**, 146805 (2006).
[7] F. V. Tikhonenko, D. W. Horsell, R. V. Gorbachev, and A. K. Savchenko, Phys. Rev. Lett. **100**, 056802 (2008).
[8] E. McCann and V. I. Fal'ko, Phys. Rev. Lett. **108**, 166606 (2012).
[9] J. Romhányi, K. Penc, and R. Ganesh, Nat. Commun. **6**, 6805 (2015).
[10] F. Wang and Y. Ran, Phys. Rev. B **84**, 241103(R) (2011).
[11] W. Li, M. Guo, G. Zhang, and Y.-W. Zhang, Phys. Rev. B **89**, 205402 (2014).
[12] R. Shen, L. B. Shao, B. Wang, and D. Y. Xing, Phys. Rev. B **81**, 041410(R) (2010).
[13] Z. Lan, N. Goldman, A. Bermudez, W. Lu, and P. Öhberg, Phys. Rev. B **84**, 165115 (2011).
[14] S. Mukherjee, A. Spracklen, D. Choudhury, N. Goldman, P. Ohberg, E. Andersson, and R. R. Thomson, Phys. Rev. Lett. **114**, 245504 (2015).
[15] R. A. Vicencio, C. Cantillano, L. Morales-Inostroza, B. Real, C. Mejía-Cortés, S. Weimann, A. Szameit, and M. I. Molina, Phys. Rev. Lett. **114**, 245503 (2015).
[16] F. Diebel, D. Leykam, S. Kroesen, C. Denz, and A. S. Desyatnikov, Phys. Rev. Lett. **116**, 183902 (2016).
[17] D. F. Urban, D. Bercioux, M. Wimmer, and W. Häusler, Phys. Rev. B **84**, 115136 (2011).
[18] B. Sutherland, Phys. Rev. B **34**, 5208 (1986).
[19] J. Vidal, R. Mosseri, and B. Douçot, Phys. Rev. Lett. **81**, 5888 (1998).
[20] A. Fang, Z. Q. Zhang, S. G. Louie, and C. T. Chan, Proc. Natl. Acad. Sci. USA **114**, 4087 (2017).
[21] M. Vigh, L. Oroszlány, S. Vajna, P. San-Jose, G. Dávid, J. Cserti, and B. Dóra, Phys. Rev. B **88**, 161413(R) (2013).
[22] D. Bercioux, D. F. Urban, H. Grabert, and W. Häusler, Phys. Rev. A **80**, 063603 (2009).
[23] B. Dóra, J. Kailasvuori, and R. Moessner, Phys. Rev. B **84**, 195422 (2011).
[24] P. M. Ostrovsky, I. V. Gornyi, and A. D. Mirlin, Phys. Rev. B **74**, 235443 (2006).
[25] V. Brosco, L. Benfatto, E. Cappelluti, and C. Grimaldi, Phys. Rev. Lett. **116**, 166602 (2016).
[26] T. Ando, J. Phys. Soc. Jpn. **71**, 2505 (2002).
[27] E. H. Hwang and S. Das Sarma, Phys. Rev. B **77**, 195412 (2008).
[28] H.-Z. Lu, J. Shi, and S.-Q. Shen, Phys. Rev. Lett. **107**, 076801 (2011).
[29] H.-Z. Lu, W. Yao, D. Xiao, and S.-Q. Shen, Phys. Rev. Lett. **110**, 016806 (2013).
[30] L. E. Golub, I. V. Gornyi, and V. Y. Kachorovskii, Phys. Rev. B **93**, 245306 (2016).
[31] T. Ando and T. Nakanishi, J. Phys. Soc. Jpn. **67**, 1704 (1998).
[32] A. P. Dmitriev, V. Yu. Kachorovskii, and I. V. Gornyi, Phys. Rev. B **56**, 9910 (1997).
[33] N. S. Averkiev, L. E. Golub, S. A. Tarasenko, and M. Willander, Phys. Rev. B **64**, 045405 (2001).
[34] I. V. Gornyi, V. Yu. Kachorovskii, and P. M. Ostrovsky, Phys. Rev. B **90**, 085401 (2014).
[35] A. Fang, Z. Q. Zhang, S. G. Louie, and C. T. Chan, Phys. Rev. B **93**, 035422 (2016).
[36] A. Lagendijk and B. A. Van Tiggelen, Phys. Rep. **270**, 143 (1996).